J Mater Sci (2007) 42:4418–4427
DOI 10.1007/s10853-006-0660-0

Co-precipitation synthesis of Nd:YAG nano-powders: the effect of Nd dopant addition with thermal treatment

Eugenio Caponetti · Maria Luisa Saladino · Filomena Serra · Stefano Enzo

Received: 2 March 2006 / Accepted: 10 July 2006 / Published online: 28 February 2007

Abstract Nanopowders of Yttrium Aluminium Garnet doped with neodymium ions were obtained by the co-precipitation method from the reaction of aluminium, yttrium and neodymium nitrate with ammonia. The amount of neodymium was selected in order to produce samples of nominal stoichiometry $Nd_XY_{(3-X)}Al_5O_{12}$ (where $X = 0.006$, 0.012, 0.024, 0.048, 0.081, 0.096, 0.17, 0.19, 0.38, 0.54, and 0.72, respectively). After washing and drying, the hydroxide precursors were subjected to Thermo-Gravimetry and Differential Thermal Analysis experiments from room temperature up to 1500 °C, which showed the presence of exothermal events accompanying phase transformation phenomena. X-ray diffraction investigations conducted with a high-resolution powder diffractometer on the specimens arrested at selected temperature of the thermograms, evidenced the amorphous-to-crystalline transformation phenomena leading to the garnet phase as the main product. On increasing the concentration of Nd, the presence of the monoclinic $Y_4Al_2O_9$ phase was also detected together with a variable amount of a metastable hexagonal $YAlO_3$ phase. Precise determination of the cubic garnet lattice parameters as a function of the neodymium content according to the Rietveld method shows a change from the value of 12.016 (±2) Å when $X = 0$ up to 12.128 (±2) Å for $X = 0.720$ with two distinctive regimes of increase. The line broadening analysis of X-ray profiles after correction for instrumental factors indicates that the average crystallite size is in the range 50–80 nm. Field-Emission Gun-Scanning Electron Microscopy observations showed the presence of aggregation features in the powders with a rounded morphology and a relatively uniform and narrow particle size distribution, with the average size figures in substantial agreement with the diffraction analyses.

E. Caponetti · M. L. Saladino
Dipartimento di Chimica Fisica and INSTM-Udr Palermo, Viale delle Scienze, Parco D'Orleans II pad.17, Palermo 90128, Italy

F. Serra · S. Enzo (✉)
Dipartimento di Chimica and INSTM-Udr Sassari, University of Sassari, via Vienna n. 2, Sassari 07100, Italy
e-mail: enzo@uniss.it

Introduction

The Czochralski single crystal fabrication technique is now a well-established technology in optics for solid-state laser production once it is doped with a rare-earth element such as neodymium [1]. However, the neodymium concentration in Yttrium Aluminium Garnet (YAG) single crystals can hardly exceed ~1 at.% [2]. It is believed that YAG ceramics prepared by chemical methods can accept a concentration of Nd atoms about 10 times higher than using the Czochralski technique, suggesting a potential for large optical absorption and gain coefficient, with consequent rewards for development of high power miniature and microchip lasers [2]. So, in alternative to the single crystal approach, polycrystalline YAG powders doped with neodymium are currently being synthesized by several chemical routes such as sol-gel [3, 4], coprecipitation of various precursors [5–7], liquid feed-flame spray pyrolysis [8] etc.

Crystallization kinetics and pathways of YAG without addition of Neodymium were studied by Johnson and Kriven [9] using a combination of

Differential Thermal Analysis (DTA), X-ray Diffraction (XRD) and Transmission Electron Microscopy (TEM). On the other hand, Gandhi and Levi [10] reported on the phase selection in precursor-derived yttrium aluminium garnet and related Al_2O_3–Y_2O_3 composition. They found that the YAG phase field was metastably extended away from its stoichiometry, as indicated by a systematic increase of the garnet lattice parameter as a function of total Y_2O_3 content. Because of the various preparative techniques used, limited attention has been paid in the literature to the influence of the dopant in the host structure of YAG and this has prompted us for a systematic investigation of the lattice parameter variation that may be induced by doping YAG with varying degree of neodymium atoms. We have recently reported the structural evolution of YAG powders doped with 5 at.% of Neodimium $Nd_{0.15}Y_{2.85}Al_5O_{12}$ from hydroxide precursors calcined at different temperatures [11] following the method used by other authors [12, 13]. It was confirmed that the crystallization process was fully accomplished at 900 °C for 1 h. The refined value of the lattice parameter after a Rietveld analysis turned out to be 12.056 (±2) Å larger than 12.016 (±2) Å obtained for the pure YAG powder [11], due to the partial substitution for Y^{3+} sites with Nd^{3+} cations.

In this paper we probe the degree of solubility of neodymium atoms in the yttrium aluminum based oxide matrix and inspect systematically the effect of thermal treatment at high temperature on the phase stability of crystallization products of the coprecipitated powders by using the Rietveld method for the analysis of the X-ray diffraction patterns. Particular concern is dedicated to the lattice parameter expansion of the cubic garnet phase as a function of neodymium content. This is an important issue in order to provide new transparent nanocrystalline Nd:YAG ceramics with unconventionally high Nd content. In addition to this, the structural features of the system will be inspected according to the isothermal nature of the annealing treatment in comparison to the continuous scanning mode.

Experimental

Materials

$Y(NO_3)_3{\cdot}6H_2O$ (Aldrich, 99.9%), $Al(NO_3)_3{\cdot}9H_2O$ (Aldrich, 98%) and Nd_2O_3 (Sigma-Aldrich, 99.99%) were the sources of Y^{3+}, Al^{3+} and Nd^{3+} ions, respectively. Solutions of ammonia (E. Merck 25%) and nitric acid (Aldrich, 90%) were prepared using all chemicals as received and adding conductivity grade water.

Preparation Nd:YAG precursors.

The Nd:YAG nanopowder precursors (aluminium, yttrium and neodymium hydroxides) were prepared by the method previously used [11]. $Y(NO_3)_3{\cdot}6H_2O$ and $Al(NO_3)_3{\cdot}9H_2O$ were dissolved in deionised water, Nd_2O_3 was dissolved in dilute nitric acid. Aqueous solutions of yttrium, aluminium and neodymium nitrates were mixed in such a way the quantity of neodymium atoms with respect to total yttrium plus neodymium atoms was 0.2, 0.4, 0.8, 1.6, 2.7, 3.2, 6.4, 12.8, 18 e 24 at.%. This is supposed to lead oxide compounds with nominal stoichiometry $Nd_XY_{(3-X)}Al_5O_{12}$ (where $X = 0.006$, 0.012, 0.024, 0.048, 0.081, 0.096, 0.17, 0.19, 0.38, 0.54 and 0.72). The hydroxides were precipitated by drop-wise addition of 5 M ammonia solution until a pH equal to 8 was reached. The gelatinous precipitate was filtered and washed with water to remove residual ammonia and nitric ions and finally with ethanol. The precipitate hydroxides were oven dried at 50 °C. The gelatinous precipitate has been filtered and washed with water several times in order to remove residual ammonia and nitrate ions. Ammonia and nitrate ions were checked by using concentrated hydrochloric acid and by the brown ring test, respectively. Finally, the precipitate has been washed with ethanol in order to facilitate the drying process.

Methods

Thermo-Gravimetry and Differential Thermal Analyses (TG-DTA) were conducted using a Setaram instrument from room temperature up to 1500 °C at an heating rate of 20 °C/min in air. After reaching the final temperature, the specimens were immediately cooled down. In addition to the TG-DTA isochronal analyses, the powders were also subjected to five cumulative stages of isothermal treatments as specified below.

Stage 1: 1 h at 900 °C;
Stage 2: same as for 1 + 1 h at 900 °C;
Stage 3: same as for 1 + 1 h at 950 °C;
Stage 4: same as for 3 + 1 h at 1000 °C;
Stage 5: same as for 4 + 1 h at 1050 °C.

Powder X-ray diffraction (XRD) patterns were recorded with a Philips PW 1050/39 diffractometer in the Bragg-Brentano geometry using Ni filtered Cu K_α radiation ($\lambda = 1.54178$ Å). The X-ray generator worked at a power of 40 kV and 30 mA and the resolution of the instrument (divergent and antiscatter

slits of 0.5°) was determined using α-SiO_2 and α-Al_2O_3 standards free from the effect of reduced crystallite size and lattice defects. The powder patterns were analyzed according to the Rietveld method [14] using the programme MAUD [15] running on a personal computer.

The lattice parameter determination in a cubic system by manual methods is generally accomplished by plotting the value a_{hkl} calculated from the position of the *hkl* line times $\sqrt{h^2 + k^2 + l^2}$ vs $\cos\theta\cot\theta$ and extrapolating to $\cos\theta\cot\theta = 0$ the resultant a_o figure [16]. In general, for cubic and non-cubic phases the same correction can be made straightforward, while maintaining a high degree of precision, in a whole powder pattern approach like the Rietveld method, which is able to correct and adjust the data for the zero offset (in our case few hundredths of degree), keeping into account simultaneously all the *hkl* that are generally distributed over the accessed angular range. As it concerns the precision of the method, of course this depends from the precision of the goniometer and suitability of data collected in relation to the angular range investigated, which in turn determines the number of *hkl* reflections inspected. Line broadening effects due to crystallite size reduction and lattice strain increase (for which the program accounts by parametric Voigt functions) may bias only slightly the determination of peak position, so that the precision normally attained in the lattice parameters so achieved can be ca. 2×10^{-5}.

Field Emission Gun-Scanning Electron Microscopy (FEG-SEM) investigations have been performed using a LEO 1530 instrument. Micrographs were obtained using an accelerating voltage of 10 kV. Energy Dispersive X-ray (EDX) measurements have been performed by a Scanning Electron Microscope **(**Philips XL30**)** equipped with an EDX device working at an accelerating voltage of 25 kV. In both studies samples were supported on the stubs by carbon paints and coated with gold.

Results and discussion

The relative homogeneous composition of each sample after stage 3 has been assessed by EDX spectra recorded from 0 to 18 keV on different sampling areas. As an example, the EDX spectra of specimens with neodymium amount of 3.2, 6.4, 12.8, 18 and 24 at. % after stage 3 are reported in Fig. 1. It is possible to recognize the peaks of all constituent elements of the sample, including carbon from stub and the gold of coating. On increasing the nominal Nd content it has been observed a concomitant increase of the area of Nd peaks (Lα, $L_{\beta 1}$, $L_{\beta 2}$, $L_{\gamma 1}$) in all specimens. A quantitative analysis of Nd, Al and Y peaks was performed on three different areas of samples. The obtained mean values confirmed the nominal Nd content calculated from the amount of reagents used in the preparative procedure.

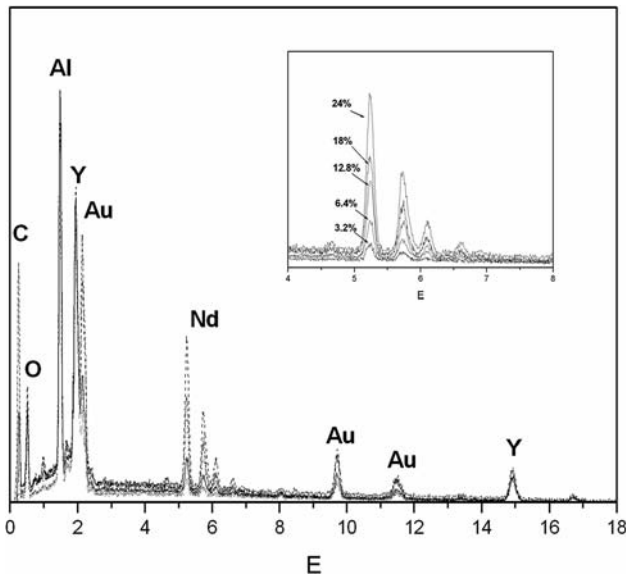

Fig. 1 EDX spectra of Nd:YAG nanopowders after the stage 3 at different neodymium content. Note that the carbon line C derives from carbon stub, while gold peaks are due to the specimen coating for microscopy observations. The quantitative elemental analysis has been performed through normalisation of neodymium, yttrium and aluminium metal lines, Nd, Y, Al respectively. In the inset the increase of the Nd peaks area with nominal neodymium content is reported

Scanning isochronal thermal treatments

The TG and DTA thermograms of precursor powdered samples oven dried at 50 °C before any treatment (isochronal, scanning mode) are reported in Fig. 2a, b, respectively. As expected, in Fig. 2a, a weight loss is observed for all the samples here examined that can be attributed to the dehydration process of the Y and Al hydroxides. Of course, the weight loss is less pronounced for samples with higher neodymium content where, at parity of metal moles involved, the initial mass is heavier. Moreover the loss appears to be terminated at 500 °C. Later, an almost constant weight is observed up to the temperature of 1500 °C.

Palmero et al. [17] have reported weight loss traces of YAG powders synthesized using a reverse-strike precipitation of chlorides into diluted ammonia. Their thermograms showed a weight loss of about 30–40% with respect to the original gel mass extended up to

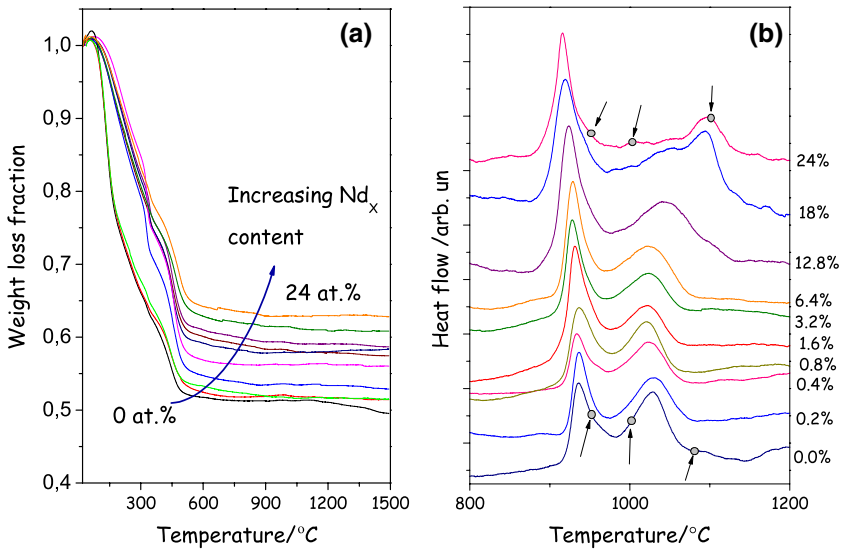

Fig. 2 (**a**) Thermogravimetry weight-loss traces of yttrium aluminium coprecipitated powders doped with increasing amount of neodymium. After a weight fall-off until 500 °C, the loss approaches a steady value and its percentage is systematically lower in specimens with higher nominal neodymium loading; (**b**) The correspondent heat flow curves show complex exothermic events due to the structural rearrangements to which the powders are subjected in this temperature range

around 900 °C. This was attributed to the progressive stripping of OH groups from the suspected amorphous precipitate. Several other papers have reported TG-DTA thermograms of gel obtained by soft chemical methods [18–20]. As reported in [11], the evolution of diffraction patterns of an yttrium aluminum dried precipitate, which was prepared according to the present procedure as a function of annealing temperature, has shown that the amorphous-to-crystalline transformation occurred in the temperature range from 700 to 800 °C. Concerning the DTA traces, there are endothermic events associated to weight loss phenomena of the reacting matrix at temperatures lower than 500 °C that are not treated in detail here.

In Fig. 2b one sees the exothermic effects recorded across the temperature range 850–1200 °C for the corresponding curves of Fig. 2a. We can devise at least two main events, whose peaks location seems to depart one from the other as a function of the neodymium content of samples. In particular, for the undoped and low-neodymium content samples, the first event shows a maximum at ca. 940 °C, while the second is located at around 1030 °C. However, the specimens with high neodymium loading (18 and 24 at.%) show the occurrence of the two events around 915 and 1110 °C respectively, suggesting a structure change of the reacting matrix (initially amorphous) likely affected by the consistent presence of the rare earth element.

Two partially overlapping exothermic events were observed around 900 and 1000 °C by Palmero et al. [17] in their undoped YAG samples. The differences from our correspondent figures for the undoped specimen can be ascribed to different protocols in sample storage and scanning rate adopted in TG-DTA experiments.

In order to assess the operative transformation mechanism during exothermic processes, we have subjected the undoped powder sample to a isochronal heating procedure up to the selected temperature values of 950, 1000 and 1080 °C labeled with circles in the trace of Fig. 2b, and then inspected the relevant XRD patterns. The diffraction data points are reported in Fig. 3 (dots) together with the Rietveld fits (full lines). The agreement between experiment and model is generally evaluated by various relative indices for the goodness-of-the-fit such as R_{wp}, (in many cases below 6%) and/or R_B (below 5%) as well as by the distribution of residuals that are expected to be uniform and

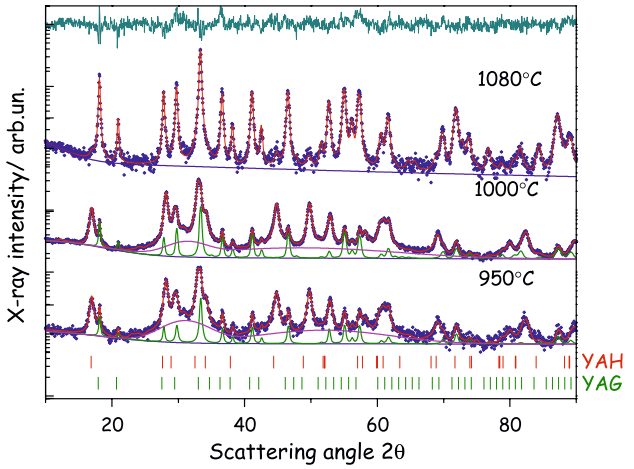

Fig. 3 XRD patterns (experimental data points as dots) of coprecipitated, undoped, yttrium aluminium oxide powders treated across the exothermal events of the thermogram up to the selected temperatures indicated. Full lines are the result of the total Rietveld fit and partial contribution of phases. The band of residuals relevant to the fit of the specimen treated at 1080 °C is reported at the top as $(I^{½}_{calc}–I^{½}_{expt})$

of supposed normal behavior in the case of a perfect numerical model used to account for the experimental patterns. Because of the data collection strategy with fixed time at each angular value the residuals are given at the top of Fig. 3 in terms of $I_{calc}^{½} - I_{expt}^{½}$. As we can see, the assumption of uniformity and normality for the residuals may not be always encountered, because of a varied number of reasons [14]. Nevertheless, the careful inspection of the numerical values found for the synthetic patterns of phases reported at the bottom of figure (note the logarithmic scale used) enabled us to perform an extensive structural analysis as it follows.

The patterns of specimen subjected to heating at 950 °C was described essentially in terms of two crystalline phases, namely 60 (±3) wt.% of hexagonal [17] $YAlO_3$ [S.G. $P6_3/mmc$, a = 3.667 (±2) Å; c = 10.515 (±4) Å] (YAH) and 30 (±3) wt.% cubic $Y_3Al_5O_{12}$ garnet [S. G. Fm-3m, a = 12.026 (±2) Å] plus an amorphous component [10 (±4) wt.%] represented by a typical diffuse profile [21, 22], suggesting that the system is still in a non-equilibrium condition. Note that the simulation of the two crystalline components included some lattice distortion in terms of anisotropic line broadening and strain according to Popa [23] in order to account closely for the experimental pattern.

A questionable point with the present analysis concerns the chemical composition of the specimen calculated from the stoichiometry of the crystallographic compounds, that appears to be different from the nominal values (confirmed by EDX) used for the preparation. For this scope, recently Laine et al. [24] have indexed a new hexagonal phase of composition $Y_3Al_5O_{12}$ with lattice parameters a = 7.36 and c = 10.52 Å, i.e., with cell size volume four times larger than the ''known'' hexagonal $YAlO_3$ phase. To reconcile this observation, half Y^{3+} ions were regularly substituted by Al^{3+} across the (002) planes of this hexagonal phase. The periodicity consequent to this replacement implied the occurrence of a diffraction peak at ~8.52° in 2θ. We did not observe any peak below 10° in our patterns, which seems to support the occurrence of the ''normal'' $YAlO_3$ hexagonal structure. In any case, possible stoichiometric deviations from the nominal composition, thought difficult to evaluate, may be due to substitutional disorder in the crystalline fraction and/or in the amorphous component. From the line broadening analysis of peak profiles, it turns out that the $YAlO_3$ hexagonal phase has an average crystallite size of ca 20 (±3) nm, while the remaining garnet appears spatially better developed with a correspondent average figure of 35 (±3) nm and strain concentration below 0.0001 (±1), that means almost absent with the resolution of our powder diffractometer. The pattern of undoped sample heated up to 1000 °C show that the percentage of garnet phase is only slightly increased at the expenses of the hexagonal form, while there is still need to maintain an amorphous profile above the polynomial background line. After heating the system up to 1080 °C the specimen appears completely transformed into the $Y_3Al_5O_{12}$ garnet crystalline structure. A careful evaluation of the lattice parameter supplies a value of 12.032 (±2) Å, not too different from the previous figure determined for the garnet separated at lower temperature. In the absence of an extra doping element, a slight change in the lattice parameter may be due to a change in composition, that is, of the Y_2O_3:Al_2O_3 molar ratio, which holds 3:5 in the case of a garnet structure. In addition to this, line broadening still persist above the instrument resolution, giving an average crystallite size of 50 (±7) nm and a lattice strain of ca. 0.0013 (±2).

The structural rearrangement to which the powder with 24 at.% neodymium loading are subjected once reached 950, 1000 and 1100 °C, respectively, proceeds as it may be assessed by inspection of the diffraction patterns reported in Fig. 4. As suggested by the top thermogram of Fig. 2b, the first exothermic event is almost complete at 950 °C. In addition to the comparison between experiment and refined model, for

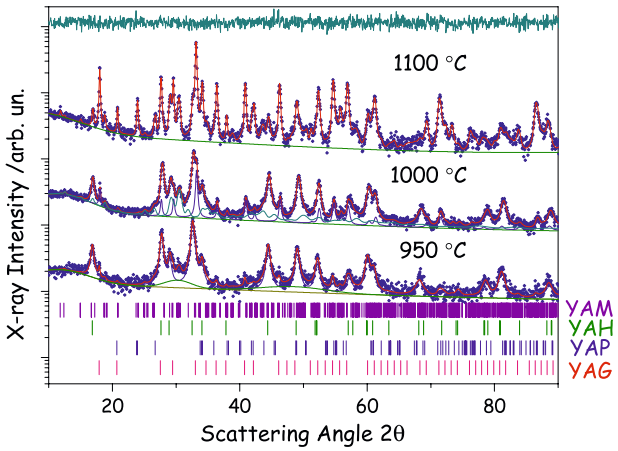

Fig. 4 XRD patterns (dots) of yttrium aluminium coprecipitated oxide powders doped with 24 at.% of neodymium, treated at the quoted temperatures. Full lines are the result of the total Rietveld fit and partial contribution of phases. The presence of neodymium seems to delay the amorphous-to-crystalline transformation process (lower curve). In the middle pattern the amorphous phase component has disappeared. The upper pattern has been resolved with the contribution of YAG, YAM, YAH and YAP phases, with a unit cell volume increased with respect to the literature values because of the presence of neodymium atoms. Note the uniform distribution of residuals for the top pattern in spite of the complexity of the system

Table 1 The quantitative phase distribution obtained with the Rietveld method in the $Nd_{0.72}Y_{2.28}Al_5O_{12}$ (Nd 24 at.%) specimen subjected to the isochronal thermal treatments in a TG-DTA furnace

Isochronal treatment of Nd:YAG (Nd 24 at.%)					
T/°C	Amorphous	YAG	YAH	YAM	YAP
950	10 (2)	4 (1)	86(3)	–	–
1000	–	18 (2)	65(3)	17(2)	
1100	–	67 (3)	10(2)	12(2)	11(2)

Phase composition is expressed in wt.%, digits in parenthesis are uncertainties on the last digits of fitting parameters. At 950 °C the metastable hexagonal YAH phase is predominant but at 1100 °C the garnet YAG phase is preferred. Note also the appearance of the monoclinic YAM phase at 1000° and that of orthorhombic YAP phase at 1100 °C

each pattern we have also reported as full lines the contribution to the total diffraction scattering due to each component phase. Table 1 reports the results of the quantitative phase determination. One sees that at 950 °C there is still a weak presence of the amorphous structure, while the major crystalline phase appears to be metastable hexagonal $YAlO_3$, accompanied by a minor amount of YAG. The absence of the amorphous component at higher scanning temperatures is expected, as well as the disappearance of the hexagonal YAH phase, simultaneously replaced by the garnet and the monoclinic $Y_4Al_2O_9$ YAM phases.

The sample heated up to 1100 °C conforms to this evolution trend, with the appearance of a further perosvkite-like $YAlO_3$ (YAP) phase [S. G. Pbnm n. 62, a = 5.250 (±4); b = 5.300 (±4); c = 7.442 (±4)]. The lattice parameters refined for the four phases of the specimen treated at 1100 °C were giving cell volumes on average 2.5% larger than the corresponding literature values of 1736.7 (±2), 203.10 (±3), 833.3 (±1) and 123.36 (±2) $Å^3$ for YAG, YAP, YAM and YAH respectively [25]. As far as the garnet structure is concerned, it is known that dodecahedral sites of yttrium are substituted for by neodymium [26] because of the similar chemistry and atomic size of elements involved. The observed increase of the cell volumes suggests that, at least for this temperature treatment, neodymium ions tend to substitute for Y in all four phases. As it concerns the microstructure properties, the fit was achieved after assuming an isotropic size-strain model for the line broadening which, in the case of the YAG phase, supplies an average crystallite size value of ca. 60 (±8) nm and a lattice strain of 0.0020 (±4) . However, in the case of YAM and YAH phases the average crystallite size is around 30 (±5) nm and the lattice strain value retrieved is 0.0035 (±7).

Isothermal treatments

For the sake of comparison with the above reported data, we have also investigated the effects of isothermal annealing the powders at 900 °C, holding time 1 h, (stage 1) followed by a further annealing at 900 °C for 1 h (stage 2). Figure 5 displays the XRD patterns of the most concentrated neodymium sample of nominal composition $Nd_{0.72}Y_{2.28}Al_5O_{12}$ (Nd = 24 at.%). The Rietveld quantitative phase analysis for the specimen subjected to stage 1 indicates (see later) that only 20 (±2) wt.% of the sample has the structure of YAG, 45 (±3) wt.% being under a monoclinic form YAM, the remaining phase being 35 (±3) wt. % of metastable hexagonal YAH. Because of the previously observed lattice expansion, our Rietveld refinement proportionally substituted for the yttrium sites of the three phases by neodymium ions in order to minimize systematic errors in the quantitative determination of the phases which stands, among other factors, from a correct account of the electron density of phases.

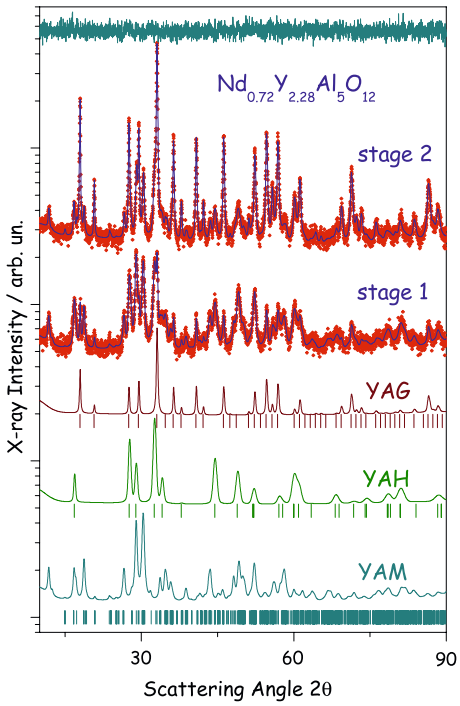

Fig. 5 The XRD patterns (dots are experimental data points) and the Rietveld fit (full lines) of the powder doped with 24 at.% of neodymium, which was subjected to the treatment stage 1 and 2 respectively. The fit to the pattern after the stage 1 was decomposed into three individual patterns of YAM, YAG and YAH phases, where the latter appears to be the most important. The relevant bar sequence of tics, reported below the synthetic patterns, mark the position expected for each peak. The pattern and fit of specimen treated as for stage 2 suggests that most of the powder is now under the form of the YAG. The band of residuals of the fit after stage 1 is reported at the top

The phase composition of the $Nd_{0.72}Y_{2.28}Al_5O_{12}$ specimen changed considerably after stage 3. In facts, the cubic YAG type phase with its 75 (±3) wt.% becomes preponderant with respect to the rest of 15 (±2) wt.% of YAM and 10 (±2) wt.% of YAH. While the lattice parameter or cell volume of the garnet phase appears unchanged with respect to the previous treatment, the values of the monoclinic and hexagonal phases are found closer to the crystallographic known lattice parameters, although they still stay on significantly different figures. The average crystallite size of the garnet phase seems attested around 80 (±15) nm, while the lattice strain appears significantly reduced, which is expected to occur after a isothermal treatment.

The morphology was also assessed by a FEG-SEM investigation on a few samples of different Nd content subjected to isothermal treatments. As an example, two representative micrographs of the Nd:YAG powder (Nd 18 % at.) after the isothermal treatment stage 3 are reported in Fig. 6. It can be observed that the particles are characterized by a rounded morphology and appear significantly agglomerated. The histogram, also shown in Fig. 6c was obtained after analysing several micrographs and depicts a relatively uniform and narrow particle size distribution. The average size of around 80 nm confirms the figures obtained from XRD line broadening analysis, suggesting that particles are monocrystals. Of course, it must be considered that electron microscopy observations are reflecting a surface mean, while the XRD results are referring to a volume weighted mean, unless coming from a Fourier Analysis of the peak profiles [27], which is not our case.

To disclose the details of the structural analysis in the coprecipitated powders after isothermal treatment stages 1, 2, 3, 4 and 5 as a function of neodymium content, a stacking of XRD patterns (log scale) is shown in Fig. 7 in the angular range from 10 to 70°. Contrary to the sample without neodymium ions, where just the YAG phase is present, in the Nd doped specimens it has observed an increased contribution of the YAM and YAH phases. According to Gandhi and Levi [10] the occurrence of the YAH hexagonal phase is not surprising because its formation at these treatment stages is facilitated by defects in the garnet structure. As mentioned earlier, possible defects in the garnet frame are arising from the consistent introduction of an excess of Nd^{3+} cation as substituent of the Y^{3+} dodecahedral sites, due to the different ionic size involved [28]. Also, in the case of off-stoichiometry, substitution of Y^{3+} for Al^{3+} in octahedral sites was detected by x-rays and optical spectroscopy in Y_2O_3-rich melt-grown single crystals of YAG and Al-Ga rare-earth garnets [29]. As a matter of fact, in a recent investigation on the synthesis and stability of $Gd_3Ga_5O_{12}$ garnet phase, it was found that an excess of Gd^{3+} cations may substitute for Ga^{3+} atoms in octahedral sites, making weak the intensity of the (220) garnet peak [30]. However, in the patterns of Fig. 5, the intensity of the (220) line profile expected at 20.80° does not change sensibly with respect to the relative value of correctly occupied Al^{3+} octahedral sites, so

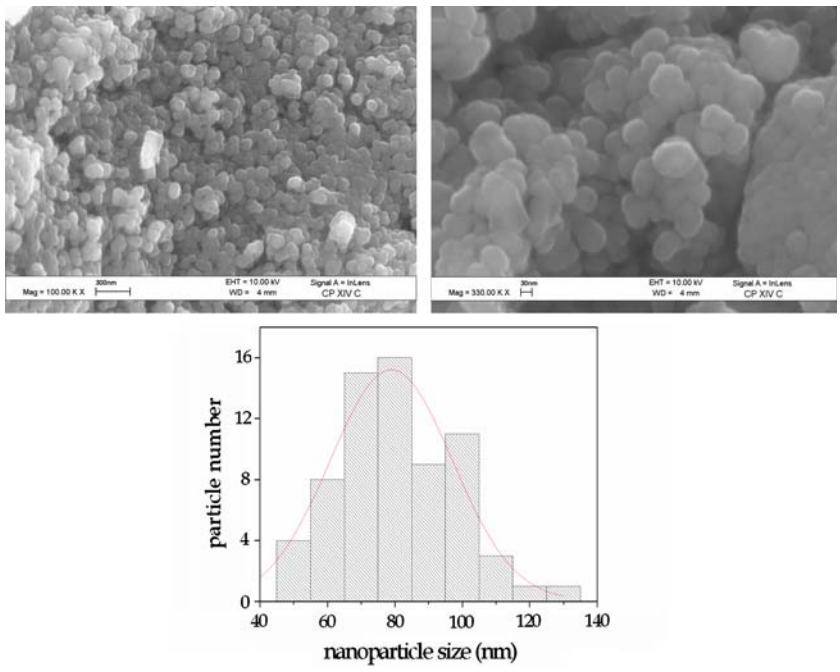

Fig. 6 Two representative micrographs of Nd:YAG doped with 18 at.% of neodymium after the stage 3 obtained by field-emission gun-scanning electron microscope. The particles are characterized by rounded morphology and appear significantly agglomerated. A careful statistics for the particle size (histogram at the bottom) supplies an average value of 80 nm

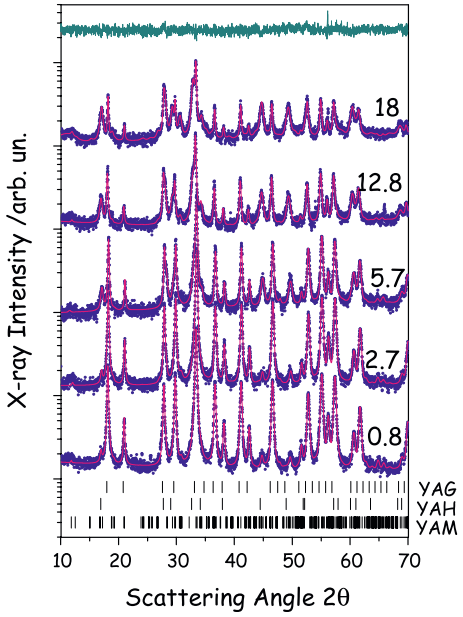

Fig. 7 The XRD patterns (dots are experimental data points) and the Rietveld fit (full lines) of the coprecipitation powders after the isothermal treatment stage 5 as a function of the neodymium content. The YAG phase decreases as a function of neodymium content in favour of the competitive formation of the YAH hexagonal and YAM monoclinic phases. The band of residuals at the top refers to the specimen with Nd 18%

this seems to exclude important off-stoichiometry in our samples, as well as substitution for Al^{3+} sites by Nd^{3+}, supporting the earlier observations of Carda et al. [31].

The results for the quantitative phase analysis for the most wanted garnet phase are reported in Table 2 for all the specimens here investigated after the five stages of thermal treatment. As mentioned before, the amount of garnet phase increases with thermal treatment but decreases on increasing the Nd content. In addition, while small but appreciable percentages of the YAM phase are recorded even for specimens with low Nd content, the metastable YAH phase is unambiguously evaluated in the XRD patterns of samples with Nd doping larger than 5.7 at.%. Moreover, the YAM phase seems to increase as a function of Nd content, but the trend is ambiguous in the case of YAH, as it can be verified in Table 3 where the quantitative evaluation of all phase products is reported for three highly concentrated specimens. One also sees that in the most concentrated Nd 24 at.% sample after stages 4 and 5, the YAH phase is absent and partially replaced by small amounts of the perovskite-like YAP phase. Although the Nd doping is contrasting the single-phasicity of powders, the increased cell volume found for all the products

Table 2 The cubic garnet phase content after evaluation of XRD patterns using the Rietveld method

Garnet phase content after isothermal treatments					
Nd at.%	Stage 1	Stage 2	Stage 3	Stage 4	Stage 5
0.8	97 (1)	99(1)	99(1)	100(1)	99(1)
1.6	96 (2)	99(1)	99(1)	99(1)	99(1)
2.7	91 (2)	97(1)	99(1)	97(1)	98(1)
3.2	92 (2)	98(1)	97(1)	98(1)	97(1)
3.8	85 (2)	94(2)	98(1)	97(1)	96(1)
5.7	77 (3)	94(2)	97(1)	97(1)	98(1)
6.4	67 (3)	92(2)	96(1)	96(1)	95(2)
12.8	58 (3)	76(3)	90(2)	92(2)	92(2)
18	37 (3)	55(3)	82(2)	87(2)	87(2)
24	20 (2)	38(3)	75(3)	82(2)	78(2)

YAG content is express in wt.%, digits in parenthesis are the uncertainties on the last digits of fitting parameters. At parity of neodymium concentration involved, the amount of the YAG phase increases on increasing the thermal treatment stage. However, the larger amount of neodymium in the coprecipitated powders seems to contrast the total YAG formation

testifies that in any case doping has been obtained for the garnet phase.

The lattice parameter behavior of the garnet phase is reported in Fig. 8 as a function of the neodymium doping amount. There is a continuous increase of the lattice parameter that can be rationalized with the insertion of large neodymium ions into the dodecahedral sites of yttrium. Moreover, a two-fold regime appears with a cross-over at the neodymium content around 6 at.%, when the increase in the lattice parameter becomes less pronounced. This can be attributed to the difficulty encountered by neodymium to replace for yttrium sites beyond a threshold value, thus favoring the precipitation kinetics of the hexagonal YAH and monoclinic YAM phases.

Conclusions

In this paper it has been proved that it is possible to prepare with a fair degree of success YAG powders doped with neodymium $Nd_XY_{(3-X)}Al_5O_{12}$ which substitutes for yttrium atoms up to the level of 24 at.%. A quantitative EDX spectra analysis of the peak area confirmed the nominal Nd content of the specimens. Selected compositions have been prepared where $X = 0$, 0.006, 0.012, 0.024, 0.048, 0.081, 0.096, 0.17, 0.19, 0.38, 0.54 and 0.72.

The kinetics study of coprecipitated powders has involved both selected heating rate and/or isothermal treatments with different holding times. After the various thermal treatments the powders have been found constituted by significantly agglomerated

Table 3 The quantitative evaluation of product distribution for the quoted neodymium concentrated samples as a function of indicated stages of isothermal treatment

Nd at.%	Nd 6.4 at.%			Nd 12.8 at.%			Nd 24 at.%			
Stage	YAG	YAH	YAM	YAG	YAH	YAM	YAG	YAH	YAM	YAP
1	67(2)	32(3)	1(0.3)	58(3)	41(3)	1(0.3)	20(2)	35(3)	45(3)	ND
2	92(2)	7(1)	1(0.3)	76(2)	22(2)	2(0.5)	38(3)	42(3)	20(2)	ND
3	96(1)	2(0.4)	2(0.4)	90(2)	5(1)	5(1)	75(3)	10(2)	15(2)	ND
4	96(1)	1(0.3)	3(0.5)	92(2)	ND	8(2)	82(2)	ND	13(2)	5(1)
5	95(1)	2(0.4)	3(0.5)	92(2)	ND	8(2)	78(2)	ND	14(2)	8(2)

Note again the appearance of the YAP phase in the $Nd_{0.72}Y_{2.28}Al_5O_{12}$ samples subjected to stage 4 and 5 respectively. Phase composition is expressed in wt.%, numbers in parenthesis are the uncertainties on the last digit of fitting parameters

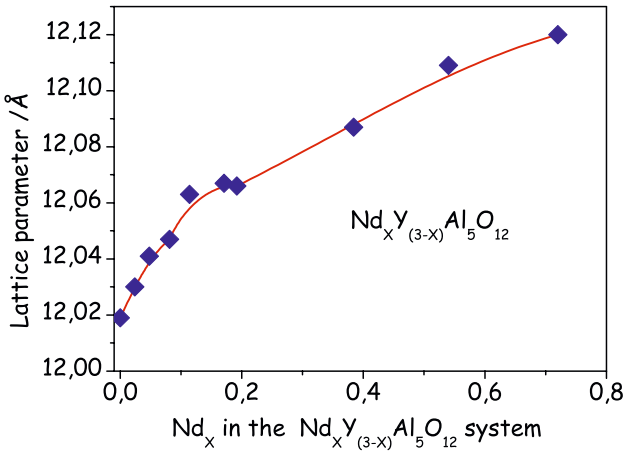

Fig. 8 The lattice parameter behaviour of the YAG phase as a function of neodymium content. Two distinct regimes are visible in the figure. The symbol size gives an idea of the evaluation of the lattice parameter

particles characterized by a rounded morphology and a size distribution in the range from 40 to 120 nm. These general features changed only slightly with Nd content.

For the specimens subjected both to isochronal and isothermal stages of treatment from 900 to 1100 °C, the neodymium doping effected an expansion of the unit cell size of the garnet from 12.02 to 12.12 Å approximately, according to a two-fold regime. The high neodymium loading seems to make difficult the conversion of the amorphous matrix to a single YAG phase, given the appearance of other yttrium aluminium oxide metastable phases like YAH and YAM. The YAP phase also appears to be induced for the highly concentrated neodymium specimens subjected to isochronal or isothermal treatment around 1050–1100 °C. Because of this phase heterogeneity of products, at present we are investigating the possibility to make further homogeneous the amorphous reacting matrix by ball milling in order to maximize the garnet formation also for samples heavily doped with neodymium. In addition to this, a further study is needed at temperatures higher than 1100 °C to verify the metastability of the YAG phases doped with sensible amounts of neodymium as in the present case as well as the possible occurrence of competitive reactions, which may stabilize other products. These studies are in progress and will be reported at a later stage.

Acknowledgements This work is carried out within two collaborative Projects, entitled "Nanostructured Luminescent Oxides", and "Synthesis of nanopowders assisted by microwaves" respectively, funded by the Italian Ministry for Education, University and Science (PRIN call 2003). We acknowledge useful discussions with prof. G. Cocco, L. Schiffini (Univ. of Sassari, Italy) and prof. M. Baricco (Univ. of Torino, Italy) on the phase metastability.We thank Dr. G. M. Ingo and Tilde De Caro (ISMN-CNR Montelibretti, Roma, Italy) for FEG-SEM micrographs, Dr. P. Guerra (Dipartimento di Ingegneria Chimica dei Processi e dei Materiali—Univ. of Palermo, Italy) for EDX analysis and Dr. Luca Lutterotti for making available a copy of the programme MAUD running in a personal computer. (http://www.ing.unitn.it/~luttero/).

References

1. Katsurayama M, Anzai Y, Sugiyama A, Koike M, Kato Y (2001) J Cryst Growth 229:193
2. Ikesue A (2002) Opt Mater 19:183
3. Ravichandran D, Roy R, Chakhovskhoi AG, Hunt CE, White WB, Erdei S (1997) J. Lumin 71:291
4. Leleckaite A, Kareiva A (2004) Opt Mater 26:123
5. Sim S-M, Keller KA, Mah T-I (2000) J Mater Sci 35:713
6. Guang Li J, Ikegami T, Lee J-H, Mori T. Yajima Y (2000) J Eur Ceram Soc 20:2395
7. Chen T-M, Chen SC, Yu C-J (1999) J Sol State Chem 144:437
8. Marchal J, Hinklin T, Baranwal R, Johns T, Laine RM (2004) Chem Mater 16:822
9. Johnson BR, Kriven WM (2001) J Mater Res 16:1796
10. Ghandi AS, Levi CG (2005) J Mater Res 20:1017
11. Caponetti E, Saladino ML, Chillura Martino D, Pedone L, Enzo S, Russu S, Bettinelli M, Speghini A (2005) Solid St Phenom 106:7
12. Wang H, Gao L, Niihara K (2000) Mat Sci Eng A288:1
13. Hsu WT, Hu W, Lu C (2003) Mat Sci Eng B104:40

14. Young RA (ed) (1993) The Rietveld Method, University Press, Oxford
15. Lutterotti L, Gialanella S (1998) Acta Mater 46:101
16. Wagner CNJ (1966) In: Cohen JB, Hilliard JE (ed) Local Atomic Arrangements studied by X-ray Diffraction, Met Soc Conf, vol 36. Gordon & Breach, New York, p 219
17. Palmero P, Esnouf C, Montanaro L, Fantozzi G (2005) J Eur Ceram Soc 25:1565
18. Chung B-J et al (2003) J Ceram Process. 4:145–150
19. Li J-G, Ikegami T, Lee J-H, Mori T (2003) J Am Ceram Soc 83:961
20. Li J-G, Ikegami T, Lee J-H, Mori T, Yajima Y. (2000) J Eur Ceram Soc 20:2395
21. Hess NJ, Maupin GD, Chick LA, Sunberg DS, McCreedy DE, Armstrong TR (1994) J Mater Sci 29:1873
22. Cannas C, Musinu A, Piccaluga G, Deidda C, Serra F, Bazzoni M, Enzo S (2005) J Sol State Chem 178:1526
23. Popa NC (1998) J Appl Crystallogr 31:176
24. Laine RM, Marchal J, Sun H, Pan XQ (2005) Adv Mater 17:830
25. Inorganic Crystal Structure Database http://icsdweb.FIZ-Karlsruhe.de
26. Carda J, Monros G, Escribano P, Alarcon J (1989) J Am Ceram Soc 72:160
27. Bertaut EF (1950) Acta Cryst 3:14
28. Shannon RD, Prewitt CT (1969) Acta Cryst B25:925
29. Lupei A, Stoicescu C, Lupei V (1977) J Cryst Growth 177:207
30. Bazzoni M, Bettinelli M, Daldosso M, Enzo S, Serra F, Speghini A (2005) J Sol State Chem 178:2301
31. Carda J, Monros G, Esteve V, Amigo JM (1994) J Sol State Chem 108:24